Ionic permeabilities of the human red blood cell: insights of a simple mathematical model

Stéphane Égée, Marie Postel, Benoît Sarels

▶ **To cite this version:**

Stéphane Égée, Marie Postel, Benoît Sarels. Ionic permeabilities of the human red blood cell: insights of a simple mathematical model. 2023. hal-04155871

HAL Id: hal-04155871
https://hal.science/hal-04155871

Preprint submitted on 7 Jul 2023

HAL is a multi-disciplinary open access archive for the deposit and dissemination of scientific research documents, whether they are published or not. The documents may come from teaching and research institutions in France or abroad, or from public or private research centers.

L'archive ouverte pluridisciplinaire **HAL**, est destinée au dépôt et à la diffusion de documents scientifiques de niveau recherche, publiés ou non, émanant des établissements d'enseignement et de recherche français ou étrangers, des laboratoires publics ou privés.

Ionic permeabilities of the human red blood cell: insights of a simple mathematical model

Stéphane Égée[*], Marie Postel[†], Benoît Sarels[†,*]

July 7, 2023

Abstract

We are interested in the system of ion channels present at the membrane of the human red blood cell. The cell, under specific experimental circumstances, presents important variations of its membrane potential coupled to variations of the main ions' concentration ensuring its homeostasis.

In this collaborative work between biologists and mathematicians a simple mathematical model is designed to explain experimental measurements of membrane potential and ion concentrations. Its construction is presented, as well as illustrative simulations and a calibration of the model on real data measurements. A sensitivity analysis of the model parameters is performed. The impact of blood sample storage on ion permeabilities is discussed.

1 Introduction

1.1 Biological motivation

Erythrocytes or red blood cells (RBCs) have evolved to optimize two functions: the transport of oxygen from lungs to the tissues, and the reverse transport of carbon dioxide. This work is carried out by three highly specialized molecules: i/ hemoglobin pigment which binds oxygen where its partial pressure is high and releases it where partial pressure is low, ii/ a cytoplasmic carbonic anhydrase which catalyzes the reversible hydration of CO_2 and iii/ a powerful Cl^-/HCO_3^- anion exchanger, a membrane protein called band 3 or SCLC4A1.

The latter is a key element of the Jacob-Stewart cycle which by exchanging HCO_3^- ions for Cl^- allows an efficient transport of CO_2 within venous blood (up to 95%) as bicarbonate ions. Thus, resting membrane potential is dictated by Cl^- conductance. For the sake of simplification, we can say that all the other

[*]Sorbonne Université, CNRS, Laboratory of Integrative Biology of Marine Models (LBI2M), Station Biologique de Roscoff (SBR), F-29688 Roscoff, France

[†]Sorbonne Université, CNRS, Université Paris Cité, Laboratoire Jacques-Louis Lions (LJLL), F-75005 Paris, France

membrane transporters are geared to maintain the constancy of volume and elastic properties, in others words to maintain homeostasis. However, keeping constant the volume of a bag with a high hemoglobin concentration is not an easy task; the colloidosmotic pressure (mainly due to the high negatively charged hemoglobin content) would tend to swell and lyse any water-permeable cell which is the case of RBCs that possess numerous water permeable pore aquaporins. Thus, the general strategy that RBCs have adopted to prevent bursting, is to maintain a very low membrane permeability to cations, particularly Na^+ the most abundant extracellular solute. The minor residual cation leaks can be balanced by the sodium and calcium pumps with only minute metabolic demands. Among the membrane transporters, ion channels have the greatest dissipative power and can transport millions of ions per second. Another feature of the ionic channels is their non-electroneutral nature, which, when activated, will cause, at least transiently, a change in membrane potential. Red blood cells have two types of cation channels. A potassium channel activated by intracellular Ca^{2+} concentration (the Gárdos channel, KCNN4) and non-selective cation channels. To date, two of these channels have been molecularly identified with certainty (the PIEZO1 channel and the TRPV2 channel). These non-selective cation channels are permeable to calcium and are therefore potentially capable of opening the Gárdos channel indirectly (See Figure 1). However, we have been able to show that such activity directly generates a transient activation of the Gárdos channel [2]. Furthermore, it is certain that during ageing, whether in vitro (storage for transfusion purposes) or in vivo (upon cell aging and senescence prior removal from the circulation), the activity of these channels would be potentially more important and could compromise cellular homeostasis by dissipating the electrochemical gradients maintained by the pumps [1, 11]. However, this activity, which can be assimilated to a leak, is difficult to quantify at the spontaneous resting potential of the cells. Indeed, at the resting potential (-12 mV), the cations taken as a whole are at equilibrium and therefore the currents generated are of relatively low intensity or at least would be masked by the predominance of the chloride conductance. However, once the Gárdos channel is activated, a hyperpolarisation follows which tends membrane potential towards the Nernst equilibrium potential for K^+ (denoted E_K in the sequel) but drives the chlorides and cations (Na^+ and K^+) away from their respective equilibrium potentials. Therefore, the intensity of the currents and thus their influence on the membrane potential can be measured by analysing the repolarisation rate and kinetics. Such conditions can be achieved by pharmacological activation of the Gárdos channel by increasing membrane permeability to Ca^{2+} using a calcium ionophore (A23187, 10µM, Figure 2). In these series of experiments, cells, kept at 4°C in their own plasma for one week, are subjected to a massive calcium influx and the evolution of the membrane potential is followed for 15 minutes. Changes in membrane potential measurements are obtained using the MBE (Macey, Bennekou, Egée) method [7] which relies on the proton distribution (see Appendix A for details).

The membrane potential drops sharply from -12 mV to values tending towards the potassium equilibrium potential due to K^+ efflux through the Gárdos channels.

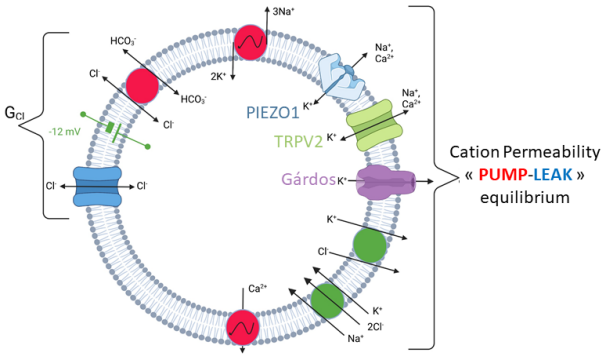

Figure 1: Red blood cell set of most important membrane transporters. The figure illustrates the main transporters involved in fluxes. Arrows indicate the direction of net fluxes for each transporter. The left-hand side of the figure describes the system that maintains the membrane potential close to the equilibrium potential for Cl^- (-12mV), comprising the Cl^-/HCO_3^- exchanger and a chloride channel. The other transporters are cationic transporters. On the one hand, the two essential red blood cell pumps, the $3Na^+/2K^+$ ATPase pump and the plasma membrane calcium pump, which consume ATP to enable transport against concentration gradients. One the right-hand side are represented the secondary active transports, which use the gradients built by the pumps to transport ions through the chemical or electrochemical gradient. The two main electroneutral transporters (KCl and NKCC cotransporter) are shown in dark green, as are the three cation channels identified yet in the red blood cell. The Gárdos channel or KCNN4, the PIEZO1 channel and more recently the TRPV2 channel. The latter two are non-selective cation channels that are not only permeable to Na^+ and K^+ but also to calcium.

Then the membrane gradually repolarises by the joint effects of the non-selective cationic and chloride conductances present at the red cell membrane.

The next Figure 3 displays the statistics of the membrane potential and provides some insight on the interpretation of Figure 2. The resting membrane potential in the upper left panel is the initial value of the potential, at rest before the opening of the potassium channel. It is labeled E_{init} in the numerical section (see Table 2). The maximum hyperpolarization denoted $\min E$ is displayed in the upper center panel. It is the minimum membrane potential reached shortly after the channel opening. The final E is measured at 15 minutes just before lysis. It is interesting to note that the difference between $\min E$ and E_0 is not monotonous with age, although less so than $\min E$ alone.

In addition to measurements of changes in membrane potential, it is fairly easy to measure intracellular Na^+ and K^+ concentration under the same experimental conditions (see appendix A for details).

Figure 4 displays the evolution of Na^+ (blue) and K^+ (orange) concentrations.

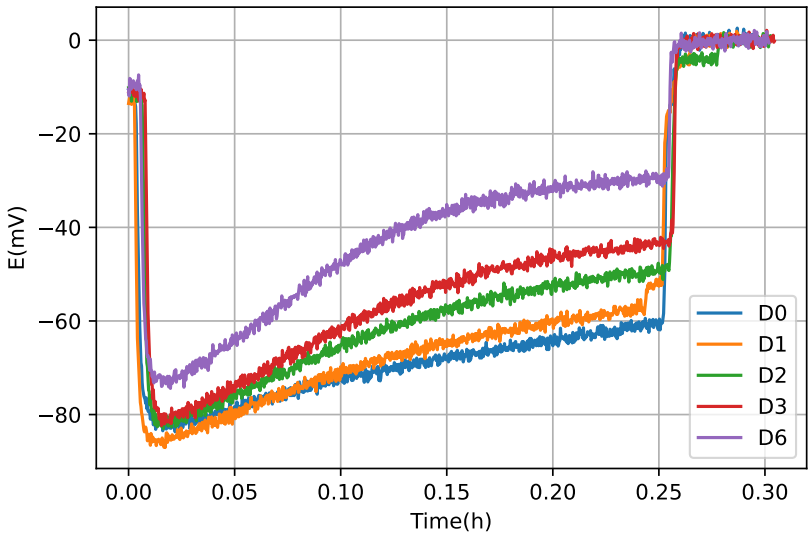

Figure 2: Raw membrane potential data after different storage durations (in days in the legend). D0 denotes fresh blood. The drug A23187 is introduced once the potential has stabilized around the chloride Nernst equilibrium, at about -12mV. At the end of the experiment the cells are lysed and the potential instantly rises back to 0 mV.

Left panel shows the changes in concentration upon 21 days of storage shedding light on the cation leak occurring upon storage at 4°C. These data will provide initial data for our model. Right panel shows the evolution of cation contents up to 4 hours, in the same conditions used in Figure 2. Only data from day 0 are available. Note that the time sampling is uneven and much coarser -about 10 minutes- than for the membrane potential which is sampled in seconds but only up to 15 minutes.

1.2 Review of the existing models

The first attempt at modeling the complex system of transport across the erythrocyte membrane has emerged in the 1980s [10]. It takes into account most of the biochemistry and the electrochemistry of the cell known at that time, and aims at covering needs and applications in physiology and pathophysiology of the red blood cell. Mathematically speaking, it is a differential-algebraic system of equations in dimension 11. In it, H^+, Na^+, K^+ and Cl^- fluxes are modeled and the kinetics of the different solutes concentrations can be computed, along with the variations of the membrane potential and the cell pH. However, new experimental setups have shown that a cationic conductance path participates to

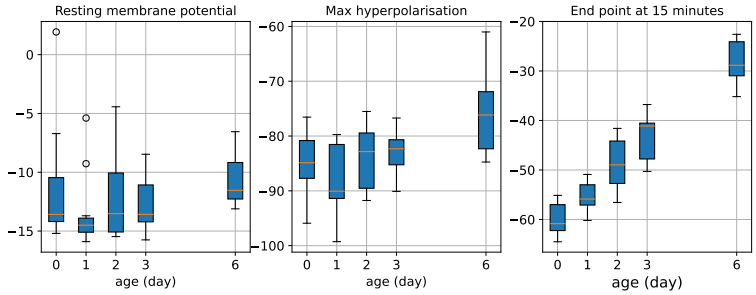

Figure 3: Statistics of data main features. The resting membrane potential is the initial condition at equilibrium before introduction of the drug. The max hyperpolarisation is the minimum potential reached once the K^+ have exited the cell. The end point is the potential reached just before the end of the experiment. Unit for the three graphs is mV.

electrolytes exchanges (Na^+, K^+, Ca^{2+}) as soon as the membrane equilibrium is disrupted. This is taken into account in a more recent version of the model [13]. In this iteration, the model is even more complex. and requires about 40 parameter values.

The models that we referred to above have - for us - two main issues. The first is that none of them is amenable to mathematical analysis, even as basic as the study of equilibria. Likewise, understanding the role and influence of the parameters is beyond our reach. This is a problem since we would want, for instance, to make a sensibility analysis and/or confront the outputs of the model with our experimental measurements. Therefore, our work is a return to the roots of electrophysiology, which puts the importance of the membrane potential back in the spotlight, and concentrates on the major time varying features.

In the next Section 2, we derive our model, a system of ordinary differential equations in dimension 4. In Section 3, we illustrate its main features with numerical simulations, showcasing two cases of interest: the one with constant permeabilities, and the one with variable permeabilities.
In Section 4, we calibrate our model with the available biological data, validate the method with a sensitivity analysis and propose a biological interpretation of our results. A number of technical details have been deferred in the appendix to preserve readability, like the experimental acquisition setup, the derivation of the objective function gradient as well as the extensive numerical tests performed to test identifiability and sensitivity.

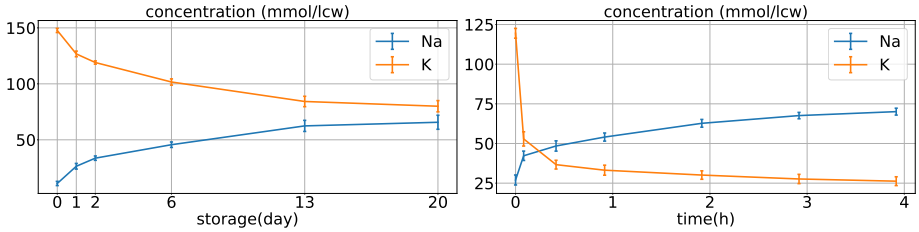

Figure 4: Concentrations $[K]$ and $[Na]$. Left: Evolution of intracellular K^+ and Na^+ concentration of RBCs stored up to 21 days in their own plasma. Results show a symmetrical leak of K^+ and Na^+ indicating that permeability not anymore compensated by Na-pump at 4°C exist in RBC membrane. Right: Changes in K^+ and Na^+ intracellular concentrations after challenging RBCs with massive Ca^{2+} entry by A23187 (10µM) injection. After a massive loss of K^+ through Gárdos channel, immediate Na^+ entry occurs that prolongs at least up for 4h.

2 Construction of the mathematical model

Our aim is to write a simple model, that will involve as few entities as possible, but still retain the important features observed in the experimental datasets. In doing so, we deliberately depart from the models mentioned in the previous section, which share the propriety of being built of different blocks for each transport pathway. Furthermore, the central role of the membrane potential is not recognized in these models. Indeed, the membrane potential is only given by the maintenance of electroneutrality at all time.

We abstract ourselves from the chemico-physical properties of the membrane, and we only consider as key parameters the membrane permeabilities for each ion.

Let us review the fundamentals of electrophysiology with the theoretical case of a single ion, following [8]. The membrane of the cell separates the inside from the outside. A ion is an entity with a (positive or negative) charge. If there is an unbalance of charge between the two compartments, this gives rise to a potential difference E. By convention, $E = E_{\text{in}} - E_{\text{out}}$. Let us denote I the intensity of the current. When current flows, the charge difference changes, and so the potential difference as well, under the law:

$$C\frac{dE(t)}{dt} + I(t) = 0, \tag{1}$$

where C is the membrane *capacity* ($C \approx 10^{-2} F\ m^{-2}$).

The current is known through Ohm's law:

$$I(t) = g_i(E(t) - E_i),$$

with g_i the membrane *conductance* for ion i and E_i the Nernst potential for ion i.

A typical value for the membrane is $g_{\text{raw}} = 10^{-13} S\ m^{-2}$: the membrane is a good electrical insulator. The presence of ionic channels at the cell membrane allows for g_i several orders of magnitude above. Anion conductance in RBCs, for instance, is $10^{-9} S.m^{-2}$. The Nernst potential is derived through a now standard thermodynamics argument. Starting from the Nernst-Planck equation we write the equilibrium between the gradients of concentration and electric field, and integrate across the membrane to obtain

$$E_i = \frac{RT}{z_i F} \ln\left(\frac{[i]_{\text{out}}}{[i]_{\text{in}}}\right),$$

where z_i is the ion valence ($z_i = 1$ for K and Na, -1 for Cl), and $[i]_{\text{in}}$ and $[i]_{\text{out}}$ denote intra- and extra-cellular concentrations for ion i.

In the end, E is driven by the differential equation:

$$\frac{dE(t)}{dt} = \frac{g_i}{C}(E_i - E(t)) = P_i(E_i - E(t)), \tag{2}$$

with P_i the membrane *permeability* for ion i. Remark that $\frac{1}{P_i}$ has units of time: it is indeed a characteristic time for equilibrium return. As discussed in the first section, we focus here on the three ions that are most present in the cell: sodium, potassium and chloride. Each ion is allowed to cross the membrane by specific ion channels. Thus, a current exists for each. Physically, the different currents add up, modifying (1) as such:

$$C\frac{dE(t)}{dt} + I_{Na}(t) + I_K(t) + I_{Cl}(t) = 0. \tag{3}$$

Each (ion specific) current has its Ohm's law:

$$I_{Na}(t) = g_{Na}(E(t) - E_{Na}), \quad I_K(t) = g_K(E(t) - E_K), \quad I_{Cl}(t) = g_{Cl}(E(t) - E_{Cl}).$$

We can factor out $\frac{1}{C}$ and we therefore get the differential equation for E as follows:

$$\frac{dE(t)}{dt} = P_{Na}(E_{Na} - E(t)) + P_K(E_K - E(t)) + P_{Cl}(E_{Cl} - E(t)). \tag{4}$$

Following the seminal paper [3], we make the common assumption that the membrane is a homogeneous substance and that the electrical field is constant so that the transmembrane potential varies linearly across the membrane. Then we can express the current of the ion i as per the Goldman–Hodgkin–Katz flux equation:

$$\frac{d[i]_{\text{in}}}{dt} = -\frac{P_i}{V_w}\frac{z_i F E}{RT}\frac{[i]_{\text{in}} - [i]_{\text{out}} \exp\left(-\frac{z_i F E}{RT}\right)}{1 - \exp\left(-\frac{z_i F E}{RT}\right)}. \tag{5}$$

We finally obtain the following system:

$$\begin{cases} \dfrac{dE(t)}{dt} = P_{Na}(E_{Na} - E(t)) + P_K(E_K - E(t)) + P_{Cl}(E_{Cl} - E(t)), \\ \dfrac{d[Cl]_{\text{in}}}{dt} = \dfrac{P_{Cl}\alpha E}{V_w} \dfrac{[Cl]_{\text{in}} - [Cl]_{\text{out}} \exp(\alpha E)}{1 - \exp(\alpha E)}, \\ \dfrac{d[Na]_{\text{in}}}{dt} = -\dfrac{P_{Na}\alpha E}{V_w} \dfrac{[Na]_{\text{in}} - [Na]_{\text{out}} \exp(-\alpha E)}{1 - \exp(-\alpha E)}, \\ \dfrac{d[K]_{\text{in}}}{dt} = -\dfrac{P_K\alpha E}{V_w} \dfrac{[K]_{\text{in}} - [K]_{\text{out}} \exp(-\alpha E)}{1 - \exp(-\alpha E)}, \end{cases} \tag{6}$$

where $\alpha = \dfrac{F}{RT}$.

We are interested in this system of equations for $t > 0$, endowed with an initial condition $(E_0, [Cl]_0, [Na]_0, [K]_0) \in \mathbb{R}_+^4$ for $t = 0$. In the next section, we will illustrate numerically the response of our model in two cases of interest: first in the case where the permeabilities are constant in subsection 3.1, and second in the case where the permeabilities are time-dependent in subsection 3.2.

3 Model numerical simulation

3.1 Evolution of the system solution with constant permeabilities

In the simplest case where the Nernst potential, external concentrations and permeabilities are assumed to remain constant throughout the experiment, the 4-ode system (6) presents a unique equilibrium

$$\begin{cases} E^* &= \dfrac{P_{Na}E_{Na} + P_K E_K + P_{Cl}E_{Cl}}{P_{Na} + P_K + P_{Cl}} \\ [Na]^* &= [Na]_{\text{out}} e^{-\alpha E^*} \\ [K]^* &= [K]_{\text{out}} e^{-\alpha E^*} \\ [Cl]^* &= [Cl]_{\text{out}} e^{\alpha E^*} \end{cases} \tag{7}$$

where $\alpha = \dfrac{F}{RT}$.

This enables us to interpret the response of the model to a sudden increase in K permeability in the presence of permeant anions of different permeability. We start from the equilibrium state corresponding to nominal ion permeabilities $P_K = P_{Na} = 0.002\text{h}^{-1}$, and $P_{Cl} \in \{0.2, 2, 20, 200\}$ (in h^{-1}). All these 4 values are much larger than $P_K = P_{Na}$ therefore the equilibrium potential $E^* = -13.6\text{mV}$ is basically equal to the Nernst potential for Cl, $E_{Cl} = -13.58\text{mV}$. Then we mimic the opening of Gárdos channel by multiplying the potassium permeability by 10^4, bringing it to $P_K = 2\text{h}^{-1}$. This triggers the evolution of the system towards a new equilibrium. For the small value of $P_{Cl} = 0.2\text{h}^{-1}$ the potassium

becomes dominant and the equilibrium potential is equal to the Nernst potential for K $E_K = -113\text{mV}$. For the intermediate P_{Cl} values 2h^{-1} and 20h^{-1}, the equilibrium potential is intermediate between the Nernst equilibrium of Cl and K. For $P_{Cl} = 200\text{h}^{-1}$, it is almost back to the original value of the Nernst potential for Cl. Interestingly, the return to equilibrium happens basically on the same time scale in the 4 cases of P_{Cl} value.

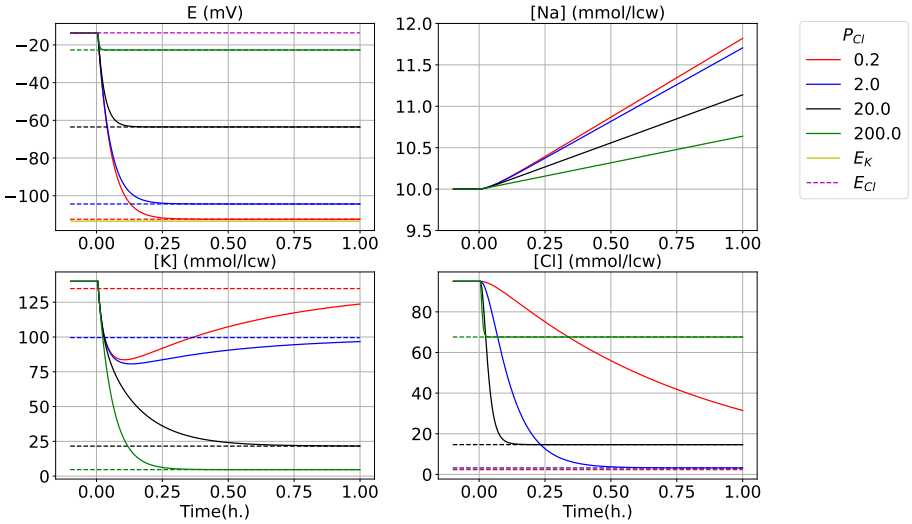

Figure 5: Response of the model to a sudden increase in K permeability in the presence of permeant anions of different permeability. Upper left : membrane potential (the magenta dashed line show the Nernst potential for potassium, the yellow line the Nernst potential for chloride), upper right : intracellular sodium concentration, lower left : intracellular potassium concentration, lower right : intracellular chloride concentration. Color code according to the anion permeability (0.2 (red), 2 (blue), 20 (black), 200 (green). The dashed horizontal lines indicate the corresponding equilibrium values after multiplying P_K by 10^4. Other parameter values are in Table 1

On the other hand the concentrations display a very different behaviour. Opening the Gárdos channel triggers the exit of potassium, as well as entrance of sodium. Consequently anion chloride exits the cell to ensure ion balance. The speed at which the three ions reach their equilibrium state is directly related to their permeability, which appears as a multiplying factor in the ODE right hand side. It also depends indirectly on the anion permeability through the dependance on E. As expected it is faster for the chloride when $P_{Cl} = 20\text{h}^{-1}$ or 200h^{-1}. If we let the simulation go on we observe that after 2 hours the potassium has reached its equilibrium - earlier for large P_{Cl}. The sodium - whose permeability has not been increased in this simulation - would reach its equilibrium thousands of hours later. The initial values for ion concentrations

are displayed in Table 1.

Parameters	Values	Unit	Description
V_w	0.75	(l/loc)	intra cellular water volume
F	96 485	C mol^{-1}	Faraday constant
R	8.314	J K^{-1} mol^{-1}	perfect gas constant
T	310	K	Temperature
α	0.037	mV^{-1}	$\alpha = \frac{F}{RT}$
$\overline{P_{Na}}$	0.002		
$\overline{P_K}$	0.002	h^{-1}	membrane ion permeabilities
$\overline{P_{Cl}}$	20		
$[Na]_{\text{out}}$	156		
$[K]_{\text{out}}$	2	mM	extra cellular concentrations
$[Cl]_{\text{out}}$	158		
$[Na]_{\text{in}}$	10		
$[K]_{\text{in}}$	140	mM	intra cellular concentrations
$[Cl]_{\text{in}}$	95		
E_{Na}	73.35		
E_K	-113.43	mV	Nernst equilibrium potentials
E_{Cl}	-13.58		

Table 1: Parameters values. $[Na]_{\text{in}}$, $[K]_{\text{in}}$ and $[Cl]_{\text{in}}$ are used as initial conditions for the concentrations in model (6).

3.2 Time variable permeability to mimic the transient nature of the channels

Opening an ion channel is a transient phenomenon. It triggers a massive entrance or exit of ions in the cell whose immediate effect is to change the membrane potential. The new value is closer to the Nernst equilibrium value of the ion which has been favoured by the channel opening. The previous numerical simulation shows that some allowance should be made to other pre existing dominant ions. The experimental data displayed in Figure 2 shows that the membrane potential drops toward the potassium Nernst equilibrium. However it does not remain at this low level, as the mathematical model would predict it, but increases again slowly. In order to enable our mathematical model to mimic this behavior, we introduce a time dependance in the ion permeabilities

$$P_i(t) = \overline{P_i} \left((M_i - 1).e^{-R_i.(t - t_{\text{inj}})} + 1 \right), \quad i \in \{Na, K, Cl\}, \quad t \geq t_{\text{inj}} \tag{8}$$

where M_i and R_i are respectively the multiplier and the relaxation coefficient for ion i, with respect to its nominal permeability $\overline{P_i}$. At the time of the injection (or channel opening) the permeability is the nominal value multiplied by M_i : $P(t_{\text{inj}}) = M_i \overline{P_i}$. If the multiplier $M_i = 1$ the permeability remains equal

to $\overline{P_i}$ at all times. If the relaxation coefficient $R_i = 0$, $P(t)$ remains equal to $P(t_{\text{inj}}) = M_i\overline{P_i}$ for all $t \geq t_{\text{inj}}$, otherwise it comes back to its nominal value asymptotically as $t \to t_{\text{inj}}$. Figure 6 displays some numerical exemples for $M_K = 10^4$ and four values for the potassium permeability relaxation coefficient. All other parameters are kept constant. The membrane potential is displayed on the right panel with the same color code as the potassium. As the potassium permeability goes back to its nominal value, the membrane potential goes back to its equilibrium value before the channel opening, $E^* = -13.6\text{mV}$, with a speed proportional to the relaxation coefficient.

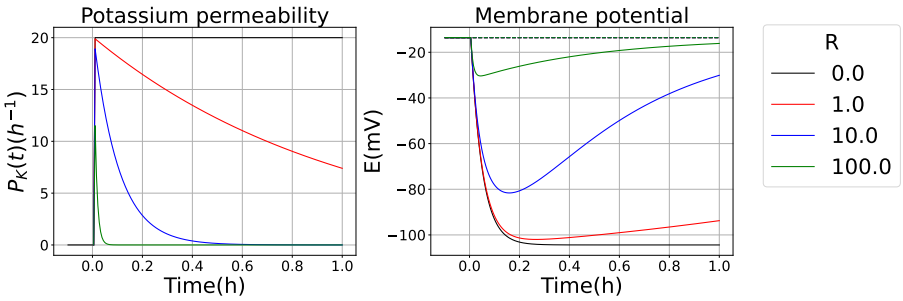

Figure 6: Time varying potassium permeability (left panel) and influence on the membrane potential (right panel) for $\bar{P}_K = 0.002h^{-1}$. The multiplying coefficient $M_K = 10^4$ and the relaxation coefficient $R_K \in \{0, 1, 10, 100\}$. Injection happens at time $t = 0$. Na and Cl permeabilities are kept constant $P_{Na} = \bar{P}_K = 0.002h^{-1}$, $P_{Cl} = 20h^{-1}$.

Having thus explored the influence of some parameters on the numerical outputs of the model, we address in the next section its adequacy to explain the available experimental data.

4 Model calibration

4.1 Calibration method

As explained in the introduction several types of measurements have been performed on experimental data. Indeed, for day 0, we are in a favorable situation where several outputs of the model, namely the membrane potential and the inner concentrations of sodium and potassium ions, can be directly confronted to experimental values. However the statistical quality of these measurements is very good for membrane potential thanks to the small time acquisition step and the redundancy made possible by several measurements on similar blood samples. In comparison the ions concentrations measurements have more a qualitative value. Furthermore, for stored samples (labeled day 1, 2 , 3 and 6) only potential measurements are available to calibrate the time dependent permeabilities.

Indeed if the permeabilities are kept constant, we have a simple explicit formula for the potential

$$E(t) = \left(E(0) - \frac{C}{S}\right) e^{-St} + \frac{C}{S},$$

where $S = \sum_{i\in\{Na,Cl,K\}} P_i$ and $C = \sum_{i\in\{Na,Cl,K\}} P_i E_i$. This implies that fitting only on potential data allows to recover only the global parameters S and C. The three ion permeabilities are not identifiable from these two values. In the case of time varying permeabilities the situation improves. We still have a formula for the potential

$$E(t) = E(0)\exp\left(\int_0^t -S(u)du\right) + \int_0^t C(s)\exp\left(\int_s^t -S(u)du\right)ds, \qquad (9)$$

since S and C now depend on time. One could hope that the non linear behavior of the permeabilities with respect to time (8) would improve the identifiability. We have not addressed this theoretical issue in this work. Indeed, discretization of (9) expresses $(E(t_i))_i$ in terms of $(S(t_i), C(t_i))_i$. If the range of values is large enough - theoretically more than 6 values, but in practice in the least square sense - can we recover the six parameters (M_k, R_k) for $k \in \{Na, K, Cl\}$ defining the $P_k(t)$?

To explore numerically this possibility we design two fit functions. The first one measure only the fit with the membrane potential

$$J(a) = \frac{\sum_{k=0}^{N}(E_a(t_j) - E_j^{\text{data}})^2}{\sum_{j=0}^{N}\left(E_j^{\text{data}}\right)^2} \qquad (10)$$

where $a \in \mathbb{R}^6$ contains the parameter values, with $a_j = M_{i_j}$ and $a_{j+3} = R_{i_j}$, for $j = 1, \ldots, 3$ and the ion ordering i_1 =Na, i_2 =K, i_3 =Cl. In (10) the times of data acquisition are denoted by

$$t_0 = t_{\text{inj}} < t_1 < \ldots < t_N = t_{\text{end}}. \qquad (11)$$

The second fit function includes two terms taking into account the fit with N_c values of sodium and potassium concentrations. We recall that unfortunately no data is available for chloride concentration.

$$\begin{aligned} J_c(a) = &\sum_{k=0}^{N} \alpha_E \left(E_a(t_j) - E_j^{\text{data}}\right)^2 + \alpha_{Na} \sum_{k=0}^{N_c} \left([Na](t_k^c) - [Na]_k^{\text{data}}\right)^2 + \\ &\alpha_K \sum_{k=0}^{N_c} \left([K](t_k^c) - [K]_k^{\text{data}}\right)^2, \end{aligned} \qquad (12)$$

with

$$\alpha_E = \frac{1}{\sum_{j=0}^{N}\left(E_j^{\text{data}}\right)^2}, \quad \alpha_{Na} = \frac{1}{\sum_{j=1}^{N_c}\left([Na]_j^{\text{data}}\right)^2}, \quad \alpha_K = \frac{1}{\sum_{j=1}^{N_c}\left([K]_j^{\text{data}}\right)^2}. \qquad (13)$$

The coefficients α_E, α_{Na} and α_K take into account the scale of each dataset and its sparsity. Indeed our choice ensures that the optimized parameters produce a good fit with the membrane potential while selecting among the various local minima the best one with respect to both the sodium and the potassium datasets.

To study the sensibility of the fit functions with respect to parameters we first generate a numerical solution of the ODE model (6), on the time interval $[0, 0.5]$, using parameters in Table 1, and coefficients of Table 3 (line 'opt') denoted in the sequel as "true values". These values will be justified in details in paragraph 4.2. We use this numerical solution as "synthetic" data and study the influence of the parameters a on $J(a)$ and $J_c(a)$ (see appendix B for details). It turns out that minimizing $J(a)$ alone is not enough to recover the parameters. On the other hand, minimizing $J_c(a)$ with $N_c = 2$, that is, including the first two concentrations at $t_c^1 = 0.083$h and $t_c^2 = 0.42$h provides a satisfactory solution, moreover robust with respect to the initial condition of the minimization strategy.

4.2 Calibration of the model using experimental data

Relying on the previous study we now turn to the numerical calibration of the model using the experimental data presented in section 1. We have five datasets for membrane potential corresponding to fresh blood and four storage durations of 1, 2, 3 and 6 days. About 900 potential values are available between $t_{\text{inj}} = 0.0036$h and $t_{\text{end}} = 0.245$h which denote respectively the time of the drug injection and the end of the experiment by cell lysis. For the fresh blood we

Parameters	Values	Unit
$\overline{P_{Na}}$	0.001518	h^{-1}
$\overline{P_K}$	0.001651	
$\overline{P_{Cl}}$	1.2	

Storage (day)	$E_{init}(mV)$	$[Na]_{\text{in}}(mM)$	$[K]_{\text{in}}(mM)$
0	-11.37	27	119
1	-12.76	26	127
2	-11.65	33	119
3	-11.36	37	115
6	-9.58	46	102

Table 2: Top table: nominal permeabilities [10]. Bottom table: resting membrane potential and initial conditions for sodium and potassium concentrations at time 0 for storage durations of 0,1,2,3, and 6 days. E_{init}, $[Na]_{\text{in}}$ and $[K]_{\text{in}}$ are used as initial conditions in (6). All the other parameter values are in Table 1.

also have some values of concentrations for Na and K ions, unfortunately on a much coarser time grid, which constitute nevertheless priceless control points. We therefore incorporate in J_c the fit with sodium and potassium concentrations at $t_c^1 = 0.083$h and $t_c^2 = 0.42$h.

We seek a minimum of $J_c(a)$ in the admissible domain defined as $D_{\mathcal{A}} = \prod_{i=1}^{6}[L_i, U_i]$ with L_i and U_i some bounds imposed to the parameters a_i from

biological considerations. Basically the permeabilities should increase at the channel opening, therefore we set $L_i = 1$ and $U_i = 10^7$ for $i = 1, 2, 3$. The relaxation factors should be some positive coefficients. Furthermore, to avoid overflows in the exponential in (8) we set $L_i = 0$ and $U_i = 10^6$ for $i = 4, 5, 6$. Starting from scratch, finding a set of parameters leading to a good fit requires many trials. Indeed some combinations of parameters randomly chosen in the admissible domain lead to very small time steps leading to unaccurate solutions of the ODE. We found it more efficient to reduce somewhat the admissible domain and to use a stochastic minimization method, CMAES[4]. This algorithm can be restarted with random seed and we found that it converges to roughly the same solution for all trials. The bounds and the optimal parameters are gathered in Table 3. The solution and the corresponding permeabilities are displayed in Figure 7. The most striking feature in this solution is the time scale difference between the sodium on the one hand and the potassium and chloride on the other hand. The abscissa have been shifted and time 0 corresponds to the injection of the drug. This is mimicked by the model by an instantaneous increase of the permeabilities, obtained by multiplying each nominal value $\overline{P_j}$ in Table 2 by its corresponding multiplier M_j in Table 3. The permeability to sodium is multiplied by 341, therefore reaching 0.51, when the permeabilities to potassium and chloride were multiplied respectively by 10^6 and 7781, reaching respectively 1731h^{-1} and 9337h^{-1}. To fit both the membrane potential and the sodium and potassium concentrations it turns out that the membrane permeabilities to potassium and chloride have to relax very quickly back to their nominal values, while the sodium behavior is much slower. Accordingly, the concentrations in ions K and Cl drop very quickly after the injection of the drug, corresponding to this very fast permeability relaxation, while the sodium concentration slowly rises.

	$M_{[i]}$			$R_{[i]}$ (h^{-1})		
	M_{Na}	M_K	M_{Cl}	R_{Na}	R_K	R_{Cl}
min	1	1	1	0	0	0
opt	341	1048931	7781	15	716	2296
max	10000	2000000	10000	10000	10000	10000

Table 3: Bounds and optimal values for parameter fit with the day 0 dataset.

In Appendix D we describe in details how the sensitivity analysis is performed, by drawing level surface for the fit functions $J(a)$ and $J_c(a)$ and computing the Sobol indices for each of the 6 parameters. Not surprisingly the parameters M_{Na}, R_{Na}, M_K and R_K which define the sodium and potassium permeabilities have a greater influence on $J_c(a)$ than the two coefficients of the chloride permeability. Indeed since no data is available for chloride concentration, these parameters influence on the fit is more indirect than the Na and K permeabilities which are directly driving the corresponding ion concentrations.

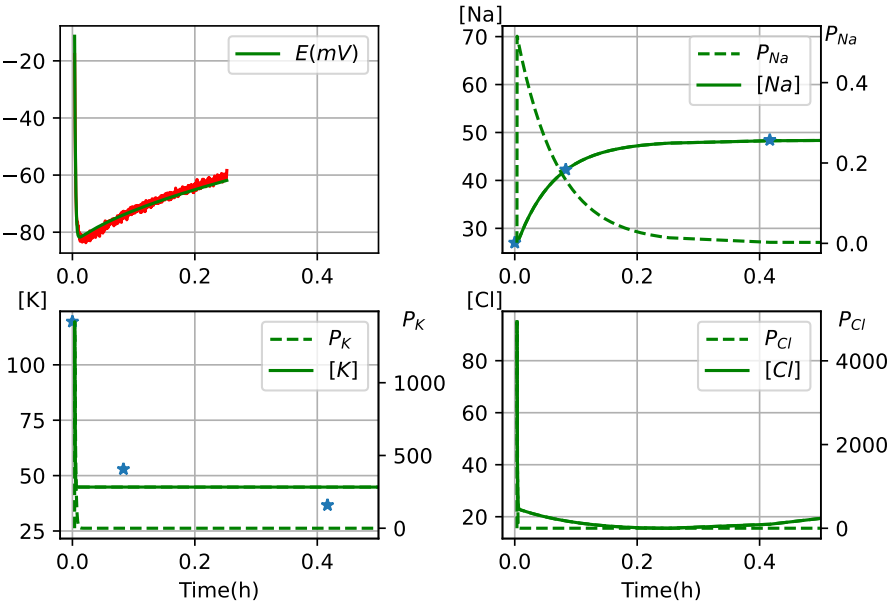

Figure 7: Best fit with day 0 dataset (no storage), obtained by minimization of fit function (12) with respect to permeability multipliers and relaxation coefficients. Data : membrane potential (in red in upper left panel), and sodium and potassium concentrations, in mmol/lcw, at $t_c^1 = 0.083$h and $t_c^2 = 0.42$h (blue stars in upper right and lower left panels). Model solution in green solid lines, scale on the left axes. The permeabilities, in h^{-1}, are plotted in dotted lines with scale on the right axes, in the same panels as the concentrations.

5 Influence of the storage duration

We now investigate the influence of the storage duration on the membrane properties. We perform a parameter identification for each available dataset, corresponding to storage of 1, 2, 3 and 6 days.

Except for time 0, which is used as initial condition for the ODE system, there are no available experimental values for $[Na]$ and $[K]$. We can therefore only use the fit $J(a)$, on the experimental membrane potential (10). For each dataset we initialize the search with the optimal parameters $p^0 = (p_i^0)_{i=1,6}$ found for the previous day, which is a good enough initial guess.

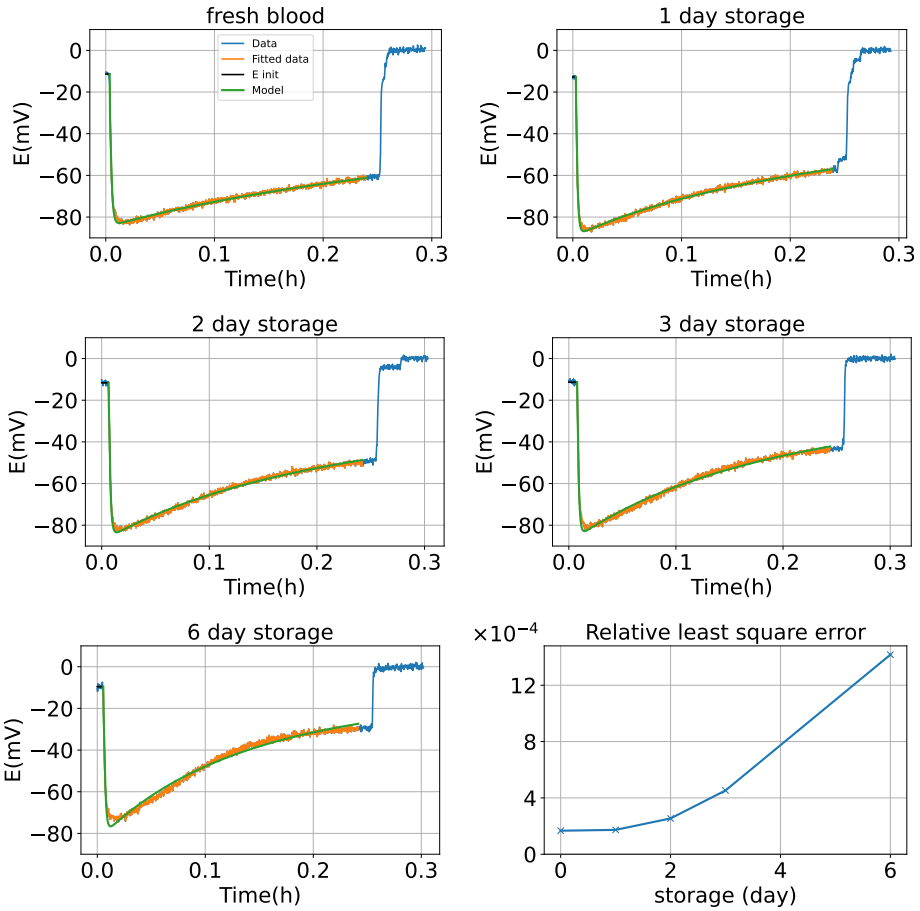

Figure 8: Best fits obtained by minimization of fit function (10) with respect to permeability multipliers and relaxation coefficients. Blue curves are the membrane potential averaged over the available datasets for a given storage duration (age). Black horizontal line over the short time range before the injection is the initial condition for the potential. Orange curves highlight the time range used in the fit function. Green curves are the model response computed with the optimal parameters. The last panel displays the relative least square error between the data and model response as a function of age.

The minimization of the fit function $J(a)$ (10) with respect to the parameter vector a is performed using the Python function `minimize` of the `scipy.optimize` package. We select the L-BFGS-B algorithm which is well suited to bounds constrained problems [15]. Of note, the upper bound for M_{Cl} has been increased to 50000. This algorithm performs better when the gradient of the objective function is provided. From the definition (10) it is obvious that computing $\nabla J(a)$ requires the derivatives of the model output with respect to a.

These are obtained by solving the ODE system obtained by differentiating (6) with respect to each parameter (see Appendix C).

	$M_{[i]}$			$R_{[i]}$ (h^{-1})			$T_{[i]}$ (h)			Error
Age	M_{Na}	M_K	M_{Cl}	R_{Na}	R_K	R_{Cl}	T_{Na}	T_K	T_{Cl}	
0	309	1048922	6516	7	666	1994	1.202	0.024	0.006	1.670e-04
1	715	1048851	11251	7	709	2972	1.364	0.023	0.004	1.730e-04
2	1032	1048667	21102	5	680	3053	1.759	0.024	0.004	2.542e-04
3	1385	1048667	21074	5	717	3426	2.042	0.023	0.004	4.530e-04
6	2488	1048666	21106	5	683	2780	2.027	0.024	0.004	1.417e-03

Table 4: Optimal parameters for each age dataset, leading to the fit displayed in Figure 8. The corresponding time variation of the permeabilities are displayed in Figure 10.

For each storage duration, the potential computed by the model, with the parameters corresponding to the best fit, is displayed in green in Figure 8 along with the experimental dataset in orange and blue. The time range entering the fit function corresponds to the orange section. The initial condition ("E init" in black in Figure 8) is set for each dataset by fitting a constant value to the potential values before the injection time, whose numerical value is found in Table 2.

The value of the fit $J(a)$ for different age datasets is displayed on the bottom right panel of this Figure 8.

To better analyse the evolution of the fit as the storage duration increases we display in Figure 9 the absolute (left panel) and relative (right panel) errors between the potential datasets and the output of the model as a function of time. Clearly there is a dominating error at the beginning of the experiment. It is due in part to the difficulty in catching the exact moment of the potential drop. This bias also comes from the fact that the potential equilibrium is not completely reached at the beginning of the experiment. In the remaining part of the experiment, where the potential rises back towards its equilibrium state, the error behaves well for short storage durations. The bias increases with the storage duration. This is an indication that our model is indeed simple and should be refined to take into account more sophisticated interactions and possibly additional influences. Nevertheless the relative errors lie within the five per cent band except for day 6 dataset of storage where it still remains beyond ten per cent.

In order to study the evolution of the model parameters with age we define a relaxation time $T_{[i]}$, for each ion $[i]$. $T_{[i]}$ denotes the time beyond which the $[i]$ ion permeability has decreased back to ten per cent of its nominal value.

$$T_{[i]} = \inf\{t \in \mathbb{R},\ t \geq t_{inj},\ P_{[i]}(t) = s\ \bar{P}_{[i]}\} \tag{14}$$

with $s = 1.1$. Using the definition of the ion permeability (8), the explicit formula

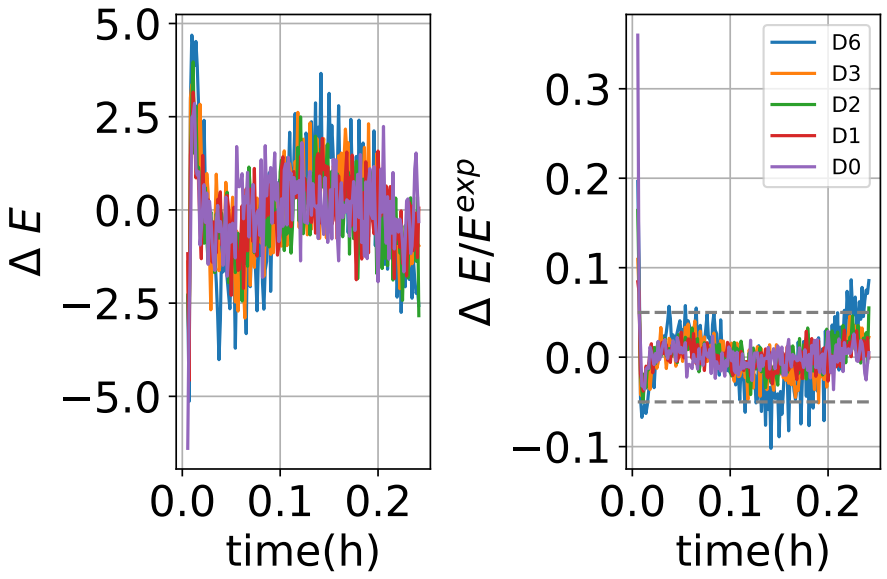

Figure 9: Absolute $E^{exp} - E(t)$ (left panel) and relative $(E^{exp} - E(t))/E^{exp}$ errors (right panel) between experimental and numerical membrane potential. Only one point every five is plotted to improve the readability of the graphs. Times have been shifted so that $t = 0$ correspond to the injection of the drug.

for $T_{[i]}$ as a function of M_i and R_i is

$$T_{[i]} \quad = \quad \max\left(0, -\frac{\ln\left(\dfrac{s-1}{M_{[i]}-1}\right)}{R_{[i]}}\right). \tag{15}$$

Figure 10 and Table 4 show that the permeabilities to potassium and chloride are not very much affected by the storage. The permeabilities to these two ions are multiplied by sensibly the same large number to mimic the injection of the drug, and they relax very fast to their nominal values, in less than 2 minutes for potassium and about 15 seconds for chloride. Note that the time scale has been blown out in the top right (K) and bottom left (Cl) panels of Figure 10 to observe the very fast decay of these permeabilities which return to their nominal values in a few seconds. Furthermore the chloride permeabilities are plotted in log scale to distinguish the differences for various days. On the contrary storage seems to influence a lot the permeability to sodium. The multiplying coefficient steadily increases with age, and the relaxation times increase, from 1.2 to 2 h. This means that for all storage durations, the permeability to sodium has not recovered its nominal value at the end of the experiment. Since the three ion

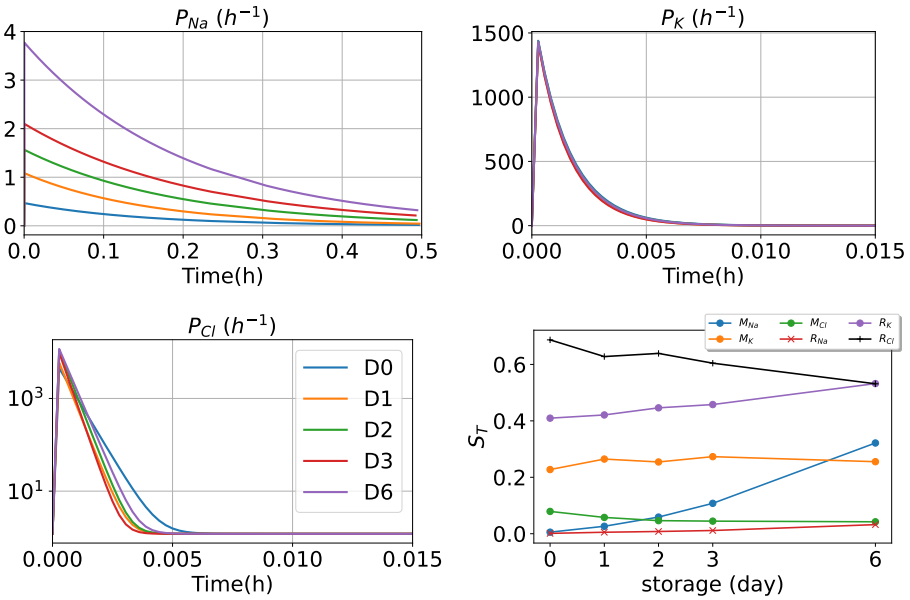

Figure 10: Time varying sodium (top left), potassium (top right) and chloride (bottom left) permeabilities for fresh blood and samples stored for 1,2,3 and 6 days. Formula (8) computed with the optimal parameters in Table 4 obtained from fitting the model for each storage duration. Times have been shifted so that $t = 0$ correspond to the injection of the drug. The bottom right panel displays the total Sobol indices of the six parameters.

permeabilities vary on very different scales, roughly 110-1000 for Na, about 10^6 for K and 10^4 for Cl, we check the sensitivity of the fit to the various model parameters in a quantitative manner, before giving biological interpretation. In Appendix D we compute the first and second order and total Sobol indices of the six parameters on the least-square fit $J(a)$ of the membrane potential with real data, for the five datasets. The bottom right panel of Figure 10 displays the evolution of the total Sobol indices as a function of the storage duration. We notice that the two parameters of K permeability, M_K in orange and R_K in violet, and the relaxation coefficient R_{Cl} in black, remain the most influential factors for all 5 fits. M_{Cl} and R_{Na} Sobol indices remain negligible. The M_{Na} amplitude coefficient in the sodium permeability (in blue), which has a negligible impact (that is lower to 0.05) on the fit with fresh blood data, becomes more and more important and has an influence comparable to M_K for the 6-day dataset.

This result indicates that Na^+ permeability must play a major role in the evolution of the response observed following activation of the Gárdos channel. It is clear that the procedure used allows maximum activation of the Gárdos channel, which remains constant throughout the 6-day of the experiment. The chloride conductance, which is already 3 orders of magnitude higher than all the

others, can vary only slightly. However, for sodium permeability, the reality is rather different. Once the hyperpolarization potential has been reached, and if we consider that the intensity of the cationic currents which will generate repolarization depends on the driving force, this is more or less identical from day 0 to day 6. This therefore implies that permeability *per se* increases over the storage time. This echoes the work carried out on the terminal density reversal phenomenon observed during the terminal senescence of red blood cells in the circulation, which become highly permeable to cations to the point of reversing the Na^+/K^+ gradient [11]. This phenomenon, combined with the present results, implies that as red blood cells age, in vivo or in vitro, inhibition of this permeability is withdrawn. It is important to note that since red blood cells have no capacity for translation and therefore no capacity to express a new set of proteins, any alteration in their permeability properties can only be attributed to intrinsic mechanisms. More importantly, the results presented here definitely point to this cationic permeability being generated by a conductive pathway. Finally, the predominance of the effect of this conductance in the repolarisation phenomenon, although it is 2 to 3 orders of magnitude lower than that for anions, can be explained by the fact that during activation of the Gárdos channel, the cell is not only totally depleted in K^+ but also in Cl^-. The latter is also rate limiting for K^+ efflux. So, even if the anionic conductance remains higher than the cationic permeability, the driving force for cations entry (Na^+) becomes the predominant one in the flux. Finally, bearing in mind that the passage of a few ions in a non-electroneutral fashion can generate a large variation in membrane potential, a simple non-selective cationic conductance whose current is no longer repressed can explain the phenomenon observed here.

6 Conclusion

On the modeling side, we found it interesting to write a simple model that puts the membrane potential back at the center of the game as in the founding papers of electrophysiology. We have proposed a time varying model for the membrane permeabilities which is coherent with the experimental set-up and relays on only two parameters per ion. The solution of the mathematical model for the membrane potential and the three ions concentrations mimics correctly the experiments. To calibrate the parameters of the model we have designed a fit function taking into account different types of datasets, membrane potential and concentrations, and performed a sensitivity analysis of the fit function with respect to the six unknown parameters. The data fit results are very good, in term of residual error - which remains below 5% except for the longest storage where it reaches 10%. The sensitivity analysis and the evolution of the permeabilities of our model with the storage duration provide interesting insights to interpret from the biological point of view the variability of the datasets.

Indeed this simple model highlights the importance of conductance pathways in membrane transport phenomena. From a more general perspective, although the terminal density reversal phenomenon has been extensively discussed in

the literature, little has been reported on long storage for transfusion purposes, where storage at 4°C also blocks the pumps. Although calcium depletion in the storage medium prevents sporadic and massive activation of the Gárdos channel, cation leak persists and significantly alters ion concentrations in red blood cells. In addition, preliminary data clearly show that overactivation of the cationic conductance(s) occurs from the first 20 days of storage and increases with time, raising the question of the fate of these cells once reinfused into patients. Knowing that the quality of transfusion bags is a major issue for the years to come, a simple measurement combined with a predictive model would make it easy to qualify transfusion bags for a safer future for patients. Finally, another neglected situation that could have major consequences is that of diabetic patients whose cells age more rapidly as a result of glycation of haemoglobin and membrane proteins. This is notably due to impairment of the Ca^{2+} ATPase pump. While the conductive nature of the permeability pathway is no longer in dispute, its capacity to be permeable to Ca^{2+} adds a further threat to the survival of red blood cells within the circulation, where a massive alteration in volume and therefore shape will definitely affect the rheological properties of the red blood cell and therefore accelerate its clearance and removal from circulation.

Several possible extensions of this model would be interesting to study. First, one possibility would be to allow the Nernst potentials to vary. In a second step, we could extend our model in dimension 5, taking into account an additional cation, in this case calcium. This would require additional precautions since calcium is present at much lower orders of magnitude, and would therefore probably require multi-scale work. Eventually, since the membrane potential experimental values exhibit strong dependance on the duration of storage, it is tempting to generalize the model to a multiscale model where the solution depends both on time and on age.

References

[1] Anne Cueff, Rachel Seear, Agnieszka Dyrda, Guillaume Bouyer, Stéphane Egée, Alessandro Esposito, Jeremy Skepper, Teresa Tiffert, Virgilio L Lew, and Serge LY Thomas. Effects of elevated intracellular calcium on the osmotic fragility of human red blood cells. *Cell Calcium*, 47(1):29–36, 2010.

[2] Agnieszka Dyrda, Urszula Cytlak, Anna Ciuraszkiewicz, Agnieszka Lipinska, Anne Cueff, Guillaume Bouyer, Stéphane Egée, Poul Bennekou, Virgilio L Lew, and Serge LY Thomas. Local membrane deformations activate ca2+-dependent k+ and anionic currents in intact human red blood cells. *PloS one*, 5(2):e9447, 2010.

[3] David E. Goldman. Potential, impedance, and rectification in membranes. *The Journal of General Physiology*, 1943.

[4] Nikolaus Hansen. The cma evolution strategy: A tutorial, 2023.

[5] Jon Herman and Will Usher. SALib: An open-source python library for sensitivity analysis. *The Journal of Open Source Software*, 2(9), 2017.

[6] Takuya Iwanaga, William Usher, and Jonathan Herman. Toward SALib 2.0: Advancing the accessibility and interpretability of global sensitivity analyses. *Socio-Environmental Systems Modelling*, 4:18155, May 2022.

[7] Julia Jansen, Min Qiao, Laura Hertz, Xijia Wang, Elisa Fermo, Anna Zaninoni, Raffaella Colombatti, Ingolf Bernhardt, Paola Bianchi, and Lars Kaestner. Mechanistic ion channel interactions in red cells of patients with gárdos channelopathy. *Blood advances*, 5(17):3303–3308, 2021.

[8] J.P. Keener and J. Sneyd. *Mathematical Physiology*. Number vol. 2 in Interdisciplinary applied mathematics. Springer, 2009.

[9] Dieter Kraft. A software package for sequential quadratic programming. *Forschungsbericht- Deutsche Forschungs- und Versuchsanstalt fur Luft- und Raumfahrt*, 1988.

[10] Virgilio L Lew and Robert M Bookchin. Volume, pH, and ion-content regulation in human red cells: analysis of transient behavior with an integrated model. *The Journal of Membrane Biology*, 92(1):57–74, 1986.

[11] Virgilio L Lew and Teresa Tiffert. The terminal density reversal phenomenon of aging human red blood cells. *Frontiers in Physiology*, 4:171, 2013.

[12] David Monedero Alonso, Laurent Pérès, Aline Hatem, Guillaume Bouyer, and Stéphane Egée. The chloride conductance inhibitor ns3623 enhances the activity of a non-selective cation channel in hyperpolarizing conditions. *Frontiers in Physiology*, 12:743094, 2021.

[13] Simon Rogers and Virgilio L. Lew. User guide to the red blood cell model (rcm), a multiplatform java-based model of human red blood cell homeostasis. *bioRxiv*, 2020.

[14] I.M Sobol. Global sensitivity indices for nonlinear mathematical models and their monte carlo estimates. *Mathematics and Computers in Simulation*, 55(1):271–280, 2001.

[15] Ciyou Zhu, Richard H Byrd, Peihuang Lu, and Jorge Nocedal. Algorithm 778: L-bfgs-b: Fortran subroutines for large-scale bound-constrained optimization. *ACM Transactions on mathematical software (TOMS)*, 23(4):550–560, 1997.

A Biological data acquisition

Changes in membrane potential measurements are obtained using the MBE (Macey, Bennekou, Egée) method [7] which relies on the proton distribution. Indeed, membrane potential can be determined indirectly by measuring the ratio of a suitable passively distributed ion. To fasten proton distribution, the CCCP protonophore (Carbonylcyanure m-chlorophénylhydrazone) is used. CCCP is a weak acid that readily permeates the membrane both as a free acid (HA) and as a free anion (A^-) and thereby acts as a proton carrier over the cell membrane. The extracellular and intracellular pH can be expressed as:

$$pH^{\text{out}} = pK_a + \log \frac{[A^-]_{\text{out}}}{[HA]_{\text{out}}},$$

and

$$pH^{\text{in}} = pK_a + \log \frac{[A^-]_{\text{in}}}{[HA]_{\text{in}}}.$$

At equilibrium, $[HA]_{\text{out}} = [HA]_{\text{in}}$ and the difference between pH_{out} and pH_{in} will reflect the anion distribution across the membrane:

$$\begin{aligned} pH^{\text{out}} - pH^{\text{in}} &= \left(pK_a + \log \frac{[A^-]_{\text{out}}}{[HA]_{\text{out}}}\right) - \left(pK_a + \log \frac{[A^-]_{\text{in}}}{[HA]_{\text{in}}}\right) \\ &= \log \frac{[HA]_{\text{in}}}{[HA]_{\text{out}}}. \end{aligned}$$

The Nernst potential for the anion is

$$E_{[A^-]} = \frac{ZF}{RT} \ln \frac{[A^-]_{\text{out}}}{[A^-]_{\text{in}}} = -61.5 \log \frac{[A^-]_{\text{out}}}{[A^-]_{\text{in}}}.$$

at 37$^{\text{o}}$C. At equilibrium the anion Nernst potential is equal to the membrane potential

$$V_m = E_{[A^-]} = -61.5 \log \frac{[A^-]_{\text{out}}}{[A^-]_{\text{in}}} = -61.5 \left(pH_{\text{out}} - pH_{\text{in}}\right).$$

As a result of a change in the membrane potential, the proton distribution will adjust and the membrane potential change is given by:

$$\Delta V_m = -61.5 \left(\Delta pH_{\text{out}} - \Delta pH_{\text{in}}\right).$$

In a completely unbuffered external medium and with a highly buffered intracellular medium, mainly from hemoglobin, the intracellular pH is practically constant. Therefore, any changes in the membrane potential can be calculated as:

$$\Delta V_m = -61.5 \Delta pH_{\text{out}}.$$

The zero potential ($pH_{\text{out}} = pH_{\text{in}}$) is obtained by addition of the detergent Triton X-100, which causes a total disintegration of the cells, and the extracellular pH attains the same value as the original intracellular pH. This method describes a way to estimate the membrane potential by measuring changes in extracellular pH, ending with the absolute calibration.

Intracellular Na^+ and K^+ concentrations are measured under the same experimental conditions, as well as cell volume, or more precisely water content as a proxy for volume. Briefly, 0.5 mL aliquots of the cell suspension were taken at each timepoint, distributed in Beckman polyethylene micro test tubes (Dutscher, France) and centrifuged at 19600 rcf for 7 minutes at 10°C. After centrifugation, the packed cell mass was separated from the supernatant by slicing the tube with a razor blade below the top of the red cell column prior weighting. For volume measurements, after weighting, the packed RBCs cells were dried to constant weight for at least 48 hours at 90°C and re-weighted. RBC volume depends on the intracellular water content, which is estimated to be about 90 fL for a healthy discocyte. Shape change can be misleading in the estimation of the cell's water content due to the great plasticity of the red cell membrane. These measurements are independent of cell shape. For Na^+ and K^+ content measurement, the packed cells within the sliced tubes were lysed in 1 mL MilliQ water. Proteins were denatured to ease separation by addition of 232 µM of perchloric acid. The tubes were spun at 12000 rcf for 7.5 minutes at $4C$ and the supernatant was passed onto sample tubes and diluted 10 times. The ionic content was measured using a flame photometer (PFP7 Jenway, France). The amounts of Na^+ and K^+ measured are reported as mmol/litre of cell water.

B Identifiability on synthetic data

In this appendix we address the identifiability of the model using only membrane potential data. We design the fit function

$$J(a) = \frac{\sum_{k=0}^{N}(E_a(t_j) - E_j^{\text{data}})^2}{\sum_{j=0}^{N}\left(E_j^{\text{data}}\right)^2} \tag{16}$$

where $a \in \mathbb{R}^6$ contains the parameter values, with $a_j = M_{i_j}$ and $a_{j+3} = R_{i_j}$, for $j = 1, \ldots, 3$ and the ion ordering i_1 =Na, i_2 =K, i_3 =Cl. In (16) the times of data acquisition are denoted by

$$t_0 = t_{\text{inj}} < t_1 < \ldots < t_N = t_{\text{end}}. \tag{17}$$

To study the sensibility of the fit function with respect to parameters we first generate a numerical solution of the ODE model (6), on the time interval $[0, 0.5]$, using parameters in Table 1, and coefficients of Table 3 (line 'opt') denoted in the sequel as "true" values. These values will be justified in details in paragraph 4.2. We use this numerical solution as "synthetic" data and compute $J(a)$ in two scenarii. First we keep the parameters M_K, R_K, M_{Cl}, R_{Cl} constant equal to the true values used to generate the "synthetic" dataset, and we let M_{Na} and R_{Na} vary in a window of 10 per cent around their true value. The left panel of Figure 11 displays the level of $J(a)$ computed in this domain. The minima of J is displayed by a white cross + which matches exactly the true position indicated by a red $\times$. Then we set M_K, R_K to one per cent higher than their true value and M_{Cl}, R_{Cl} one per cent lower, and compute $J(a)$ for M_{Na} and R_{Na} in a window of 10 per cent around their true value. We see on the right panel of Figure 11 that the minimum at the white cross +, is now far away from the true position $\times$. This is not surprising but the real bad news is that the dark blue area, where J is close to its minimum, is much larger than in the ideal case. This observation plus other numerical attempts at minimizing $J(a)$ starting from various initial conditions, convince us that without prior information, E data are not sufficient to identify the model parameters.

We therefore propose to weight the objective function by two terms taking into account the fit with N_c values of sodium and potassium concentrations.

$$\begin{aligned} J_c(a) = &\sum_{k=0}^{N} \alpha_E \left(E_a(t_j) - E_j^{\text{data}}\right)^2 + \alpha_{Na} \sum_{k=0}^{N_c} \left([Na](t_k^c) - [Na]_k^{\text{data}}\right)^2 + \\ &\alpha_K \sum_{k=0}^{N_c} \left([K](t_k^c) - [K]_k^{\text{data}}\right)^2 \end{aligned} \tag{18}$$

with

$$\alpha_E = \frac{1}{\sum_{j=0}^{N}\left(E_j^{\text{data}}\right)^2}, \quad \alpha_{Na} = \frac{1}{\sum_{j=1}^{N_c}\left([Na]_j^{\text{data}}\right)^2}, \quad \alpha_K = \frac{1}{\sum_{j=1}^{N_c}\left([K]_j^{\text{data}}\right)^2}.$$

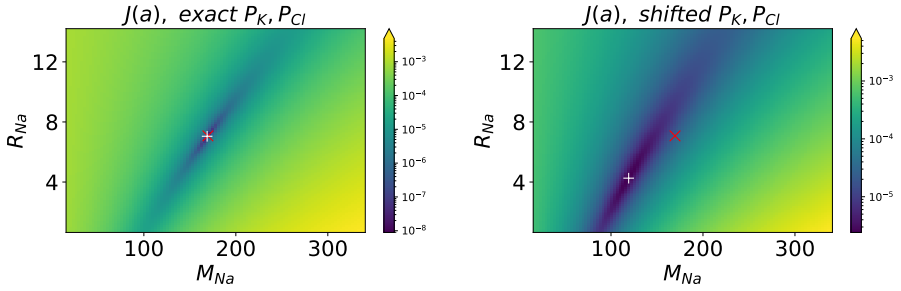

Figure 11: Level of $J(a)$ against M_{Na} and R_{Na} for experimental data obtained by simulating (6) with parameter values in Table 1. In left panel M_K, R_K, M_{Cl}, R_{Cl} are kept equal to the values in Table 3. In right panel M_K, R_K are set 1% higher, and M_{Cl}, R_{Cl} 1% lower than the values in Table 3. The minima of J is denoted by a white cross +, the true position by a red $\times$.

The coefficients α_E, α_{Na} and α_K take into account the scale of each dataset and its sparsity. Indeed they ensure that the optimized parameters produce a good fit with the membrane potential while selecting among the various local minima the best one with respect to both the sodium and the potassium datasets.

In our preliminary study using our ideal dataset we first test the behavior of $J_c(a)$ in the case where the sodium and potassium concentrations are available on the same time grid as the membrane potential. Figure 12 displays the level of $J_c(a)$ for $N_c = N$ and all things equal otherwise to Figure 11. We see on the right panel that the minimum of J_c ($\times$) remains much closer to the true location (+) than when only E is used. The vicinity of the minimum, in dark blue, is also sharper using Na and K.

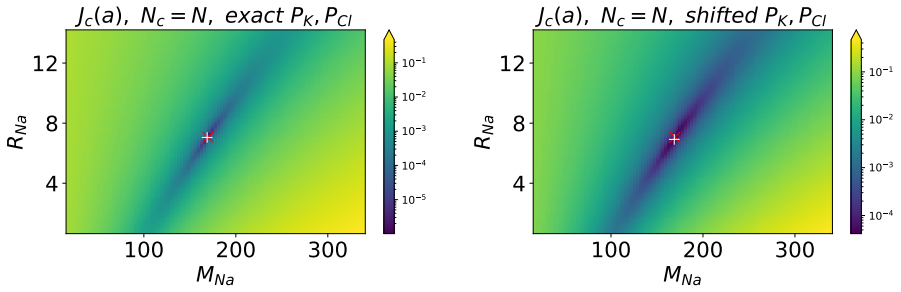

Figure 12: Level of $J_c(a)$ against M_{Na} and R_{Na} for experimental data obtained by simulating (6) with parameter values in Table 1. The minima of J is denoted by a white cross +, the true position by a red $\times$. In left panel M_K, R_K, M_{Cl}, R_{Cl} are kept equal to the values in Table 3. In right panel M_K, R_K are set 1% higher, and M_{Cl}, R_{Cl} 1% lower than the values in Table 3. In (18) $t_k^c = t_k$ for $k = 1 \ldots, N = N_c$.

We now study the realistic configurations corresponding to the available experimental data. Besides the values at $t = 0$ which are used as initial condition for the ODE system, only the first measured value at $t_1^c = 5$mn (0.083h) is in the time range of the membrane potential dataset. The second one at $t_2^c = 25$ mn (0.42h) already lies outside the time range. We will consider both cases $N_c \in \{1, 2\}$.

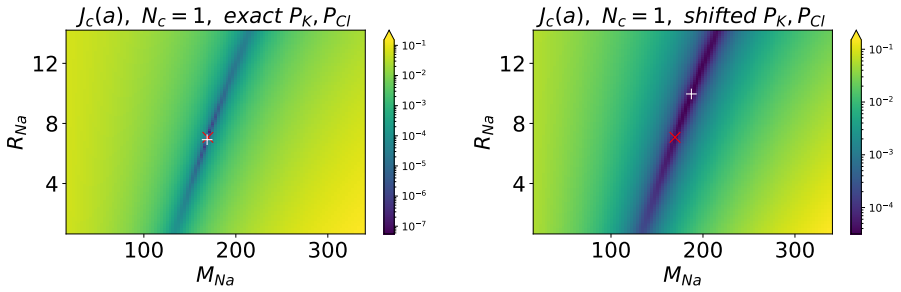

Figure 13: Level of $J_c(a)$ against M_{Na} and R_{Na} for experimental data obtained by simulating (6) with parameter values in Table 1. The minima of J is denoted by a white cross +, the true position by a red $\times$. In left panel M_K, R_K, M_{Cl}, R_{Cl} are kept equal to the values in Table 3. In right panel M_K, R_K are set 1% higher, and M_{Cl}, R_{Cl} 1% lower than the values in Table 3. In (18) $N = 896$, $t_N = 0.294$h; and only one concentration is used to match with $[Na]$ and $[K]$: $N_c = 1$ and $t_1^c = 0.083$h.

In Figure 13 we see that almost all the benefits of using Na and K data is lost if only one point is used, here the one at $t = 0.083$h, in the time range $[0, 0.25]$ of the potential dataset. The area of the minimum of J_c, in dark blue, is enlarged compared to that of Figure 12 where full concentrations datasets where used. The right panel also shows that in the case where the potassium and chloride permeabilities are shifted by 1%, the minimum of J_c misses by far the true location. This bad performance is somewhat expected, since fitting one curve through one single point is not very forceful indeed.

On the contrary Figure 14 shows that using the first two Na and K experimental data points, at $t_c^1 = 0.083$h and $t_c^2 = 0.42$h gives results as good if not better than the case where $[K]$ and $[Na]$ were available on the same grid as the potential in Figure 12.

This result seems to indicate that our weighting coefficients α_E, α_{Na} and α_K play their role of taking into account the sparsity of the experimental values of concentrations. Also compared to the results in Figure 11 the results are better: in the ideal case in the left panel, the minimum area in dark blue is sharper. In the right panel, where the K and Cl permeabilities are off by 1%, the minimum of J_c remains almost at the true location.

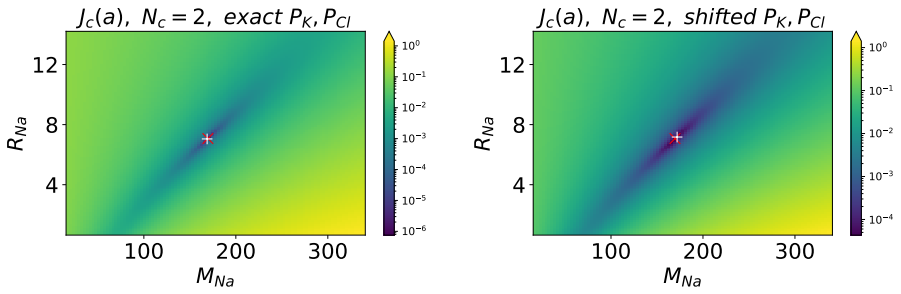

Figure 14: Level of $J_c(a)$ against M_{Na} and R_{Na} for experimental data obtained by simulating (6) with parameter values in Table 1. The minima of J is denoted by a white cross +, the true position by a red $\times$. In left panel M_K, R_K, M_{Cl}, R_{Cl} are kept equal to the values in Table 3. In right panel M_K, R_K are set 1% higher, and M_{Cl}, R_{Cl} 1% lower than the values in Table 3. In (18) $N = 896$, $t_N = 0.294$h, and two concentrations are used to match with $[Na]$ and $[K]$: $N_c = 2$ and $t_1^c = 0.083$h, $t_2^c = 0.416$h.

C Gradient of the objective function

We recall the basic method to study the dependance of a generic ODE system

$$\begin{aligned} \frac{dX(t;a)}{dt} &= F(t, X(t;a); a) \\ X(0;a) &= X_0 \end{aligned}$$

with respect to some parameters $a \in \mathbb{R}^p$ appearing in the expression of the right hand side $F : \mathbb{R} \times \mathbb{R}^m \to \mathbb{R}^m$. We denote by $X(t;a)$ the solution of the Cauchy problem for a given set of parameters. In the case where the initial condition $X_0 \in \mathbb{R}^m$ does not depend on the parameters a, the gradient of each component X_k, for $k = 1, \ldots, m$ with respect to a, is solution of the ODE system

$$\begin{aligned} \frac{d\nabla_a X_k(t;a)}{dt} &= \nabla_a F_k(t, X(t;a); a) + \sum_{j=1}^{m} \frac{\partial F_k(t, X(t;a); a)}{\partial x_j} \nabla_a X_j(t;a), \\ \nabla_a X_k(0;a) &= 0_{\mathbb{R}^p}. \end{aligned}$$

Suppose that we want to minimize a fit function

$$J(a) = \sum_{k=1}^{m} \gamma_k \sum_{n=0}^{N_k} (X_k(t_n^k; a) - X_{k,n}^{\text{data}})^2, \tag{19}$$

with respect to a (note that the time sampling may vary according to the component). The gradient

$$\nabla J(a) = 2 \sum_{k=1}^{m} \gamma_k \sum_{n=0}^{N_k} (X_k(t_n^k; a) - X_{k,n}^{\text{data}}) \nabla_a X_k(t_n^k; a),$$

will be required by the most efficient algorithms. It can be computed along with $X(t;a)$ by solving the system

$$\begin{aligned} \frac{dY(t;a)}{dt} &= G(t, Y(t;a); a), \\ Y(0;a) &= Y^0, \end{aligned}$$

where

- $Y : \mathbb{R} \to \mathbb{R}^{m \times (p+1)}$ with, for $k = 1, \ldots, m$,
  - $Y_{k+m(k-1)}(t) = X_k(t;a)$
  - $Y_{k+1+m(k-1),\ldots,k(m+1)}(t) = \nabla_a X_k(t;a)$.
- $Y^0 \in \mathbb{R}^{m \times (p+1)}$ with, for $k = 1, \ldots, m$,
  - $Y^0_{k+m(k-1)} = X^0_k$
  - $Y_{k+1+m(k-1),\ldots,k(m+1)}(t) = 0_{\mathbb{R}^p}$.

- $G : \mathbb{R} \times \mathbb{R}^{m(p+1)} \to \mathbb{R}^{m(p+1)}$ with, for $k = 1, \ldots, m$,
  - $G_{k+m(k-1)}(t, y) = F_k(t, (y_{i+m(i-1)})_{i=1,\ldots,m}; a)$
  - $G_{k+1+m(k-1),\ldots,k(m+1)}(t, y) = \nabla_a F_k(t, (y_{i+m(i-1)})_{i=1,\ldots,m}; a).+$
    $\sum_{j=1}^{m} \dfrac{\partial F_k(t, (y_{i+m(i-1)})_{i=1,\ldots,m}; a)}{\partial x_j} (y_i)_{i=j+1+m(j-1),\ldots,j(m+1)}.$

The expression of J and its gradient becomes

$$\begin{aligned} J(a) &= \sum_{k=1}^{m} \gamma_k \sum_{n=0}^{N_k} y_{k+m(k-1)}(t_n^k; a) - X_{k,n}^{\text{data}})^2, \\ \nabla J(a) &= 2 \sum_{k=1}^{m} \gamma_k \sum_{n=0}^{N_k} (y_{k+m(k-1)}(t_n^k; a) - X_{k,n}^{\text{data}})(y_j)_{j=k+1+m(k-1),\ldots,k(m+1)}(t_n^k; a). \end{aligned}$$

In our case we have $m = 4$ and

$$\begin{aligned} F_1(t, X) &= \sum_{k=1}^{3} P_{i_k}(t; a)(E_{i_k} - X_1) \\ F_{1+k}(t, X) &= -z_k \frac{P_{i_k}(t; a)}{V_w} \frac{FX_1}{RT} \frac{X_{k+1} - [i_k]^{\text{ext}} \exp(-\dfrac{FX_1}{RT})}{1 - \exp(-z_k \dfrac{FX_1}{RT})}, \text{ for } k = 1, 2, 3 \end{aligned}$$

where

$$P_{i_k}(t) = \bar{P}_{i_k} \left((M_{i_k} - 1).e^{-R_{i_k}.(t - t_{\text{inj}})} + 1 \right). \tag{20}$$

For the ion ordering i_1 =Na, i_2 =K, i_3 =Cl we have therefore $z = (1, 1, -1)$. We can rewrite the permeabilities in terms of the parameters $a \in \mathbb{R}^6$, with $a_j = M_{i_j}$ and $a_{j+3} = R_{i_j}$, for $j = 1, \ldots, 3$

$$P_{i_k}(t) = \bar{P}_{i_k} \left((a_k - 1).e^{-a_{k+3}.(t - t_{\text{inj}})} + 1 \right). \tag{21}$$

The partial derivatives of the model function F with respect to the parameters are obtained through the partial derivatives of the permeabilities

$$\frac{\partial P_{i_k}(t)}{\partial a_j} = \delta_{k,j} \bar{P}_{i_k} .e^{-R_{i_k}.(t - t_{\text{inj}})} - \delta_{k,j-3} \bar{P}_{i_k} (M_{i_k} - 1).(t - t_{\text{inj}}) e^{-R_{i_k}.(t - t_{\text{inj}})}.$$

We have then

$$\begin{aligned} \frac{\partial F_1(t, X)}{\partial a_j} &= (\delta_{k,j} + \delta_{k,j-3}) \frac{\partial P_{i_k}(t)}{\partial a_j} (E_{i_k} - x_1), \quad \text{for } k = 1, 2, 3, \text{ and } j = 1, \ldots, 6 \\ \frac{\partial F_1(t, X)}{\partial x_i} &= -\delta_{1,i} \sum_{k=1}^{3} P_{i_k}(t; a) \text{ for } i = 1, \ldots, 4 \end{aligned}$$

and for $k = 1, 2, 3$, denoting $y_1^k = \dfrac{-z_k F x_1}{RT}$ for simplicity,

$$\begin{aligned}
\frac{\partial F_{1+k}(t,X)}{\partial a_j} &= (\delta_{k,j} + \delta_{k,j-3}) \frac{y_1^k}{V_w} \frac{\partial P_{i_k}(t)}{\partial a_j} \frac{x_{k+1} - [i_k]^{\text{ext}} \exp(y_1^k)}{1 - \exp(y_1^k)} \text{ for } j = 1, \ldots, 6 \\
\frac{\partial F_{1+k}(t,X)}{\partial x_1} &= -\frac{P_{i_k}(t;a) z_k F}{V_w RT} \left(\frac{x_{k+1} - [i_k]^{\text{ext}} \exp(y_1^k)}{1 - \exp(y_1^k)} + y_1^k \frac{\exp(y_1^k)(x_{k+1} - [i_k]^{\text{ext}})}{(1 - \exp(y_1^k))^2} \right) \\
\frac{\partial F_{1+k}(t,X)}{\partial x_{j+1}} &= \delta_{k,j} \frac{P_{i_k}(t;a) y_1^k}{V_w (1 - \exp(y_1^k))}, \text{ for } j = 1, 2, 3.
\end{aligned}$$

D Sensitivity analysis

D.1 Level sets of LS fit on real data

Following the methodology in Appendix B, we study the sensitivity of the objective function with respect to the 6 parameters, in the case of the fresh blood real dataset, where we can compare the two objective functions, including or not the concentration control points.

We run three sets of numerical simulation. In each one we make vary two parameters M_i and R_i, related to one of the three ions, while keeping the four other parameters constant, equal to their optimal value for $J_c(a)$ (see Table 3).

The two varying parameters M_i and R_i cover a square window $[M_i^{opt}/10, 2M_i^{opt}]\times [R_i^{opt}/10, 2R_i^{opt}]$.

The results of the three simulations are displayed in Figure 15. We see that the range of value for $J(a)$ if at least one order of magnitude larger than for $J_c(a)$. This is normal since the fit is much better if only sought for the membrane potential, disregarding the concentrations. The value of the best fit for $J_C(a)$ is also highly dependent on the weights α_E,α_{Na} and α_K of its three additive factors.

The ratio of the maximum over the minimum values of the fit $J(a)$ within the square range is one order of magnitude lower for Na than for K or Cl. The influence of the Na permeability on the fit with the potential alone is much lower than the influence of the K and Cl permeabilities.

This is no more the case for $J_c(a)$. The influence of the Na permeability on the fit including concentrations is comparable and even larger than the influence of the K and Cl permeabilities.

ion	min J	max J	max/min J	min J_c	max J_c	max/min J_c
Na	0.00019	0.019	102	0.032	3.7	116
K	0.00032	0.60	1863	0.032	2.63	82
Cl	0.00032	0.67	2085	0.032	1.17	36

Table 5: Extremal values of $J(a)$ and $J_c(a)$ when only two parameters M_i and R_i are varying in $[M_i^{opt}/10, 2M_i^{opt}] \times [R_i^{opt}/10, 2R_i^{opt}]$.

D.2 Sobol indices of LS fit on day 0 data

In this paragraph we quantify the influence of the parameters on the fit with the data by computing Sobol indices, using the Python package SALib [5, 6]. As explained in [14] the idea is to consider the ANOVA representation of the

function of interest, here the fit function $J(a)$ (or $J_c(a)$ for that matter)

$$\begin{aligned} J(a) &= J_0 + \sum_{s=1}^{6} \sum_{i_1<\cdots<i_6} J_{i_1\cdots i_s}(a_{i_1},\cdots,a_{i_s}) \\ &= J_0 + \sum_{i=1}^{6} J_i(a_i) + \sum_{i<j} J_{i,j}(a_i,a_j) + \cdots + J_{1\cdots 6}(a). \end{aligned}$$

After rescaling the parameter domain to $[0,1]^6$ the different contributing terms can be estimated by Monte Carlo approximations of the following integrals

$$\begin{aligned} \int_0^1 J(a)da &= J_0, \quad \textstyle\int_0^1 J(a)\prod_{k\neq i} da_k = J_0 + J_i(x_i) \\ \int_0^1 J(a)\prod_{k\neq i,j} da_k &= J_0 + J_i(x_i) + J_j(x_j) + J_{i,j}(x_i,x_j) \end{aligned}$$

and their variances

$$D = \int_0^1 J^2(a)da - J_0^2, \quad D_{i_1\cdots i_s} = \int_0^1 J_{i_1\cdots i_s} da_{i_1}\cdots da_{i_s},$$

which satisfy the relation

$$D = \sum_{s=1}^{6} \sum_{i_1<\cdots<i_s} D_{i_1\cdots i_s}.$$

The ratios

$$S_i^1 = \frac{D_i}{D}, \quad S_{i,j}^2 = \frac{D_{ij}}{D}, \quad S_i^T = \frac{D_i + \sum_{j\neq i} D_{ij} + \sum_{j\neq k\neq i} D_{ijk} + \cdots}{D},$$

are respectively the first order, second order and total Sobol indices. The first-order index can be used to measure the fractional contribution of a single parameter to the output variance. Second-order sensitivity indices are used to measure the fractional contribution of two parameter interactions to the output variance. Total-order sensitivity indices take into account both the main, second-order and higher-order effects.

Note that we are not studying the influence of the parameters on the model in general, which would involve also the variation of this influence with time. Here we concentrate on the parameters leading to best fit with the fresh RBC dataset and we therefore select a range of values centered on the best fit parameters, of half width equal to 90% of the nominal value in each parameter direction. The Sobol indices are computed using a Monte Carlo sample of size $16384\times(2d+2) \approx 230000$. The 95% confidence interval are superimposed on the first order and total indices, to make sure that the sample size is large enough.

On the top panel we see the Sobol indices relative to $J(a)$, which measures the fit with the membrane potential. The first moments, in yellow on the

Param	S_p^1	$S_p^1 + \sum_{q \neq p} S_{p,q}^2$	S_p^T
M_{Na}	0.0347	0.163	0.240
M_K	0.101	0.295	0.351
M_{Cl}	0.00310	0.0181	0.0402
R_{Na}	0.120	0.282	0.362
R_K	0.148	0.447	0.518
R_{Cl}	0.0255	0.107	0.165

Table 6: Sobol indices of the six parameters for the fit function $J_c(a)$ for the fresh blood dataset.

left panel, quantify the direct influence of each of the 6 parameters on $J(a)$. The second order index, on the right panel quantify the influence of correlated parameters. Is it admitted that a parameter has a significant influence if its Sobol index is larger than 0.05. Here only M_K, R_K and R_{Cl} satisfy this criterion, as independent factors. In terms of correlations, the mutual influence of M_K and R_K and of R_K and R_{Cl} are significant. The bottom panels display the Sobol indices relative to $J_c(a)$, which measures the fit with the membrane potential and the concentration in Na and K control points. Here all parameters seem important -with the exception of M_{Cl} whose total Sobol index barely reaches 0.04. However if M_K, R_{Na} and R_K directly influence J_c; with a 1st Sobol index higher that 0.05. The mutual influences -measured by the second order index- of (M_{Na}, R_{Na}), (M_K, R_K) and (R_K, R_{Cl}) seem to be also important.

D.3 Influence of storage on Sobol indices of LS fit

A last set of numerical simulations is performed to check the observation made in Paragraph 5 that Sodium ion transfers seem to be more important as the duration of storage increases. This conclusion would be consistant with the data measurement at time 0 showing an increase in sodium concentration and a decrease in potassium concentration as the storage duration increases (see left panel of Figure 4).

Indeed the permeabilities identified by fitting the model with the membrane potential data steadily increase with age (see first panel of Figure 10), but the sensitivity analysis on the fresh blood results indicate that the sodium permeability influence on the fit with the membrane potential is negligible (See top panels of Figure 16). It is therefore important to check whether this influence remains negligible or not after the blood has been stored.

In Figures 17 and 18 we display the Sobol indices relative to $J(a)$ for the 5 available dataset of membrane potential after a storage of 0,1,2,3 and 6 days. The first moments, in yellow on the left panel, quantify the direct influence of each of the 6 parameters on $J(a)$. The total moment in red on the left panel, quantify the total influence. The second order index, on the right panel quantify the influence of correlated parameters.

Looking at the first red column in the left panels, we see that the total

influence of M_{Na}, the amplitude parameter of the Sodium permeability, increases with the storage duration and becomes comparable to the influences of M_K and R_K, which were the two predominant factors for fresh blood.

We summarize these observations in Figure 19. The influences of R_{Na}, remains negligible, while the influence of M_{Na} increases along with the duration of storage.

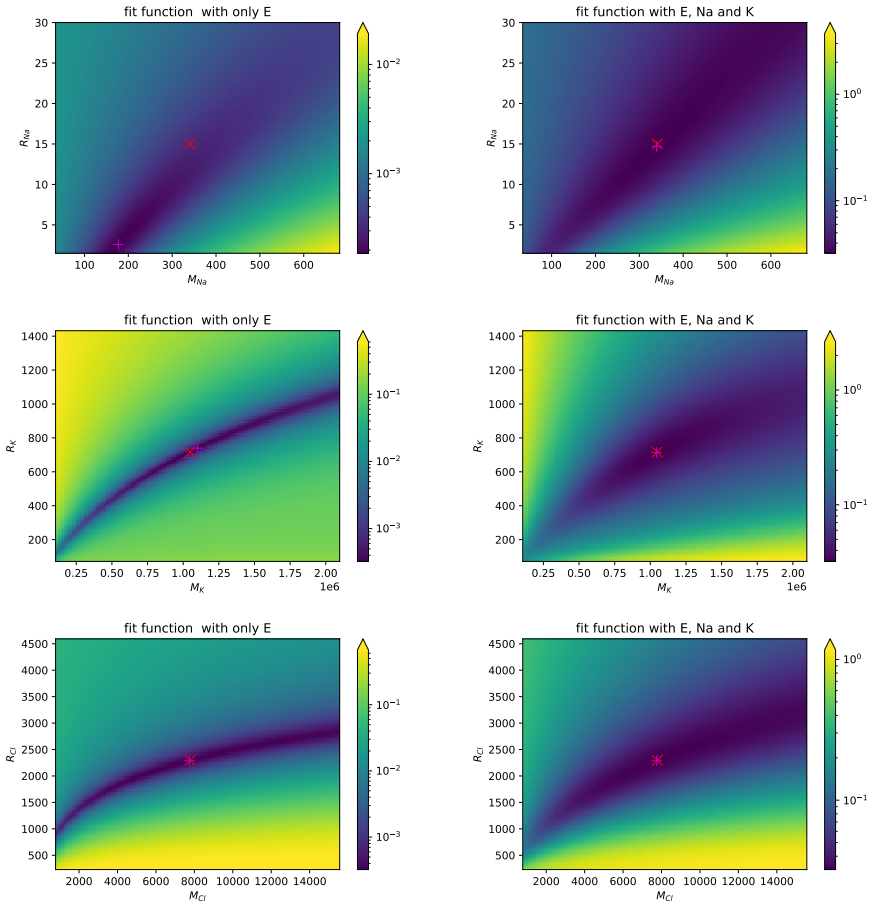

Figure 15: Level of $J(a)$ (left panel) and $J_c(a)$ (right panel) against M_i and R_i for the fresh RBC (day 0). i is Na in the top panels, K in the middle ones and Cl in the bottom ones. The parameters related to the two other ions are kept equal to their values in Table 3. The minima of J is denoted by a magenta cross $+$, the true position by a red $\times$.

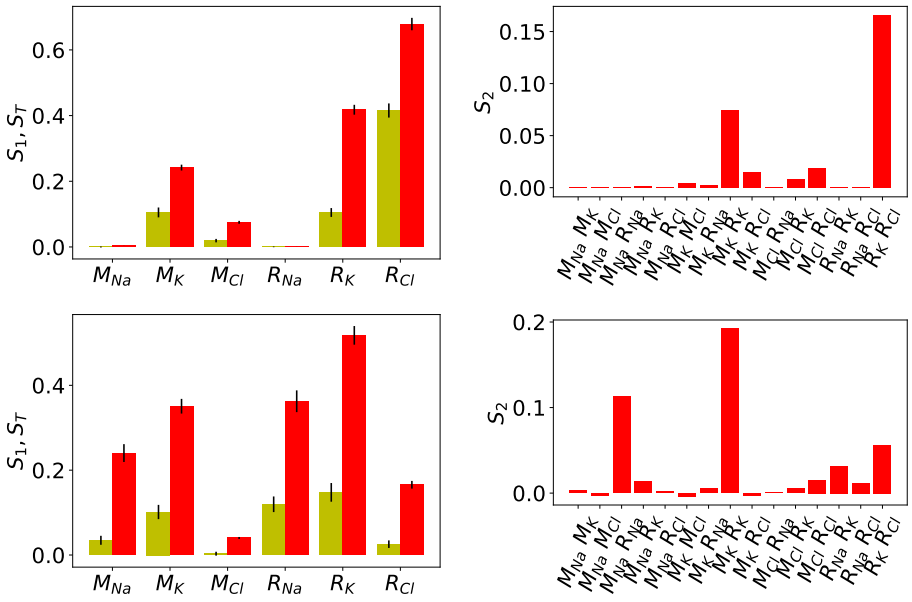

Figure 16: Sobol indices for the membrane potential fit (top panel) and for the full dataset fit (bottom panel) for fresh blood (no storage). The left bar charts display the first (yellow) and total (red) moments of each parameter. The right panel charts display the 2nd order correlations

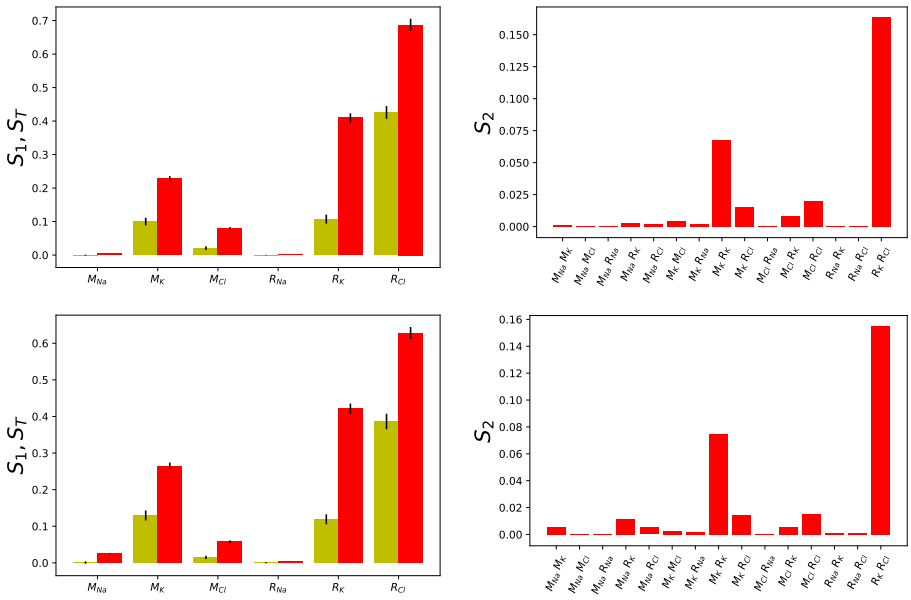

Figure 17: Sobol indices for the membrane potential fit for a storage duration of 0 and 1 days (from top to bottom). The left bar charts display the first (yellow) and total (red) moments of each parameter. The right panel charts display the 2nd order correlations

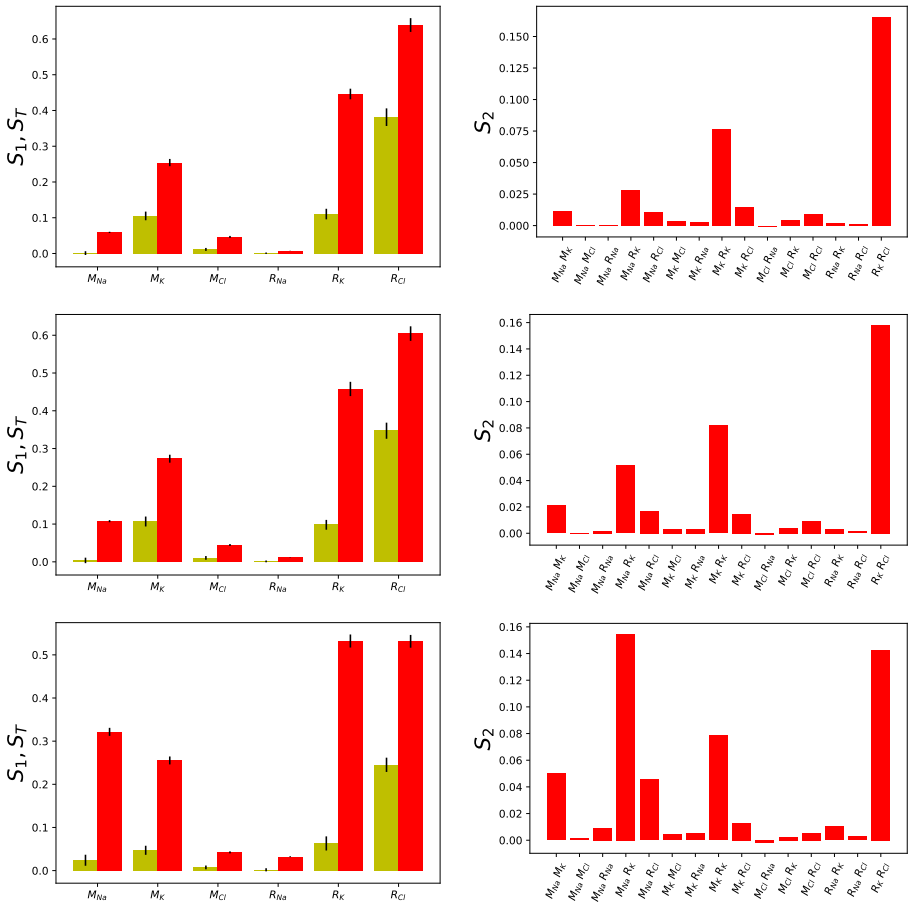

Figure 18: Sobol indices for the membrane potential fit for a storage duration of 2,3 and 6 days (from top to bottom). The left bar charts display the first (yellow) and total (red) moments of each parameter. The right panel charts display the 2nd order correlations

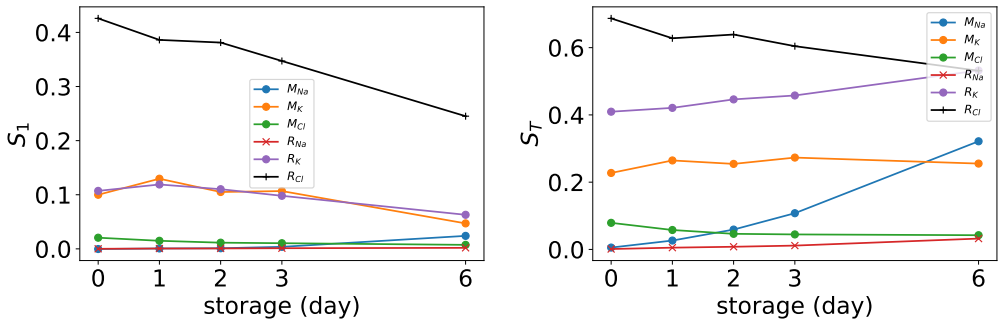

Figure 19: First order (left) and total (right) Sobol indices for the membrane potential fit as a function of storage duration. The total index for R_{Na} remains below the threshold 0.05.